Edinburgh Research Explorer

Distinguishing the Roles of Topoisomerases I and II in Relief of Transcription-Induced Torsional Stress in Yeast rRNA Genes

Distinguishing the Roles of Topoisomerases I and II in Relief of Transcription-Induced Torsional Stress in Yeast rRNA Genes[▽]

Sarah L. French,[1] Martha L. Sikes,[1] Robert D. Hontz,[2]† Yvonne N. Osheim,[1] Tashima E. Lambert,[1] Aziz El Hage,[3] Mitchell M. Smith,[1] David Tollervey,[3] Jeffrey S. Smith,[2] and Ann L. Beyer[1]*

Department of Microbiology[1] and Department of Biochemistry and Molecular Genetics,[2] University of Virginia Health System, Charlottesville, Virginia 22908-0734, and Wellcome Trust Centre for Cell Biology, University of Edinburgh, Edinburgh EH9 3JR, United Kingdom[3]

To better understand the role of topoisomerase activity in relieving transcription-induced supercoiling, yeast genes encoding rRNA were visualized in cells deficient for either or both of the two major topoisomerases. In the absence of both topoisomerase I (Top1) and topoisomerase II (Top2) activity, processivity was severely impaired and polymerases were unable to transcribe through the 6.7-kb gene. Loss of Top1 resulted in increased negative superhelical density (two to six times the normal value) in a significant subset of rRNA genes, as manifested by regions of DNA template melting. The observed DNA bubbles were not R-loops and did not block polymerase movement, since genes with DNA template melting showed no evidence of slowed elongation. Inactivation of Top2, however, resulted in characteristic signs of slowed elongation in rRNA genes, suggesting that Top2 alleviates transcription-induced positive supercoiling. Together, the data indicate that torsion in front of and behind transcribing polymerase I has different consequences and different resolution. Positive torsion in front of the polymerase induces supercoiling (writhe) and is largely resolved by Top2. Negative torsion behind the polymerase induces DNA strand separation and is largely resolved by Top1.

Eukaryotic cells have two major topoisomerases that are capable of efficiently relaxing torsionally stressed DNA: topoisomerase I (Top1) and topoisomerase II (Top2) (75). They are both abundant nuclear proteins with roles in many DNA activities, and since they both can relax positive and negative torsion, they can substitute for each other in most situations (11, 28, 29, 35, 62). In spite of this partial functional redundancy, they control DNA topology by very different mechanisms (65). Top1 (a type IB topoisomerase) makes transient single-strand breaks in torsionally stressed DNA (recognizing the torque in such DNA), followed by controlled rotation of the nicked strand and resealing of the DNA in a more relaxed state (38). Top2 (a type IIA topoisomerase) recognizes juxtaposed DNA helices (as in supercoiled DNA) and passes one DNA helix through the other by making a transient double-strand break in one of the helices (61, 65). Top2 plays an essential role during S phase because it is required to decatenate chromosomes, thus preventing their breakage and loss during cytokinesis (5). Yeast cells without Top1 grow very well, whereas cells lacking functional Top2 remain viable if they are prevented from completing mitosis (5, 11, 28, 29, 70).

Topoisomerase activity is required during RNA synthesis due to transcription-induced supercoiling of DNA, as originally described in the "twin-domain" model (46, 76). During transcription, DNA turns on its axis relative to the polymerase, with one turn of the helix every ~10.5 bp (due to the twist of

Watson-Crick DNA). If there are no topoisomerases to allow the DNA to rotate relative to the polymerase, the DNA becomes overwound (positive torsion) ahead of the polymerase and underwound (negative torsion) behind it. Polymerase I (Pol I) transcription of the ribosomal DNA (rDNA) is very active and therefore topologically demanding (11, 66). *Saccharomyces cerevisiae* has 150 to 200 copies of the 35S rRNA gene in one array, which account for ~60% of total transcription in growing cells (77). These genes have high reinitiation rates and generate long, bulky transcripts on multiple, tandemly linked genes—conditions that demand efficient topoisomerase activity to alleviate transcription-induced torsion.

Both Top1 and Top2 are found in nucleoli and are associated with initiation-competent Pol I (7, 22). They play partly redundant roles in Pol I transcription (66) and in suppression of mitotic recombination in rDNA (17). Top1, which is concentrated in nucleoli and has target sites in rDNA (9, 53, 81), has additional nucleolar roles including ribosome biogenesis (44) and rDNA silencing (13, 68). Synthetic lethal genetic interactions have been reported between yeast *TOP1* and several genes encoding proteins involved in rRNA transcription (6, 14, 26, 30, 78). In spite of these multiple indications for a role of Top1 in the nucleolus, pre-rRNA transcription is only slightly compromised in *S. cerevisiae* strains lacking Top1 as long as Top2 is present (11, 12, 23). There is, however, evidence that the rDNA has an unusual topology in *top1*Δ cells because it becomes highly recombinogenic (17), refractory to analysis by pulsed-field gel electrophoresis (18) and unusually accessible to psoralen cross-linking (15).

In yeast deficient for Top1 and Top2 activity, Pol I is able to transcribe short reporter genes but is unable to elongate through the 6.7-kb rRNA gene (11, 23, 66). This is presumably due to extreme positive torsion, which resists strand separation

* Corresponding author. Mailing address: Department of Microbiology, Box 800734, University of Virginia Health System, Charlottesville, VA 22908-0734. Phone: (434) 924-5611. Fax: (434) 982-1071. E-mail: alb4h@virginia.edu.
† Present address: Environmental Preventative Medicine Unit #2, United States Naval Base, Norfolk, VA 23511.

and can twist the DNA into positive supercoils. In the absence of only Top1, plasmid templates may be subject to high negative torsion when transcribed (12). Negative torsion can be relieved either by negative supercoiling or by unwinding of the DNA duplex, suggesting that the helix might become unwound in short regions behind polymerases (12) as has indeed been shown to occur in the C-myc promoter (39, 40). Studies on *Escherichia coli* strains deficient in topoisomerases (21) have shown that negative torsion is conducive to hybrid formation between underwound template DNA and nascent RNA. Such DNA:RNA hybrids together with the displaced nontemplate DNA strand are called R-loops. R-loops block transcription elongation (32, 71) and in bacteria are deleterious to cell viability (3, 49, 50). We have recently shown that loss of Top1 enhances R-loop formation in yeast rRNA genes concomitant with an increase in transient blocks to elongation (23).

Although many studies have used topoisomerase-deficient cells to study the role of these proteins in transcription (76), most have used reporter genes on plasmid templates. In the present study, the well-characterized rRNA genes are studied in their normal chromosomal context, and for the first time, a direct gene visualization approach is used to analyze the *in vivo* effects of topoisomerase depletion. The results show a clear distinction between the consequences of Top1 versus Top2 deficiency on active rDNA and support the recent speculation that Top1 plays the major role behind elongating polymerases, while Top2 does so in front of elongating polymerases (42). We also found that *top1Δ* cells can tolerate large regions of melted rDNA template (up to 2 kb), which is nonetheless compatible with continued transcription of the affected gene, unlike transcriptional R-loops, which block elongation (23, 32, 71). These results provide insight into the abnormal DNA topology and genetic instability found in yeast rDNA in topoisomerase-deficient strains.

MATERIALS AND METHODS

Yeast strains and growth conditions. Yeast strains were grown in YPD at 30°C unless otherwise indicated. Yeast strains used were control strains JS772 (*MATa his3Δ1 leu2Δ0 ura3Δ0*), BY4741 (*MATa his3Δ1 leu2Δ0 met15Δ0 ura3Δ0*) (10), and YB169 (BY4741 but *Tap-RFA1*::HIS3) (the present study). *TOP1* deletion strains were SY84 (BY4741 but *top1Δ*::KanM4) (79), W1854-2A (W303 but *top1Δ*::*LEU2 RAD5*) (kindly provided by Rodney Rothstein), and YB168 (BY4741 but *top1Δ*::*KanM4 Tap-RFA1*::HIS3) (the present study). Control and experimental strains for RNase H under- and overexpression were YAEH271 [BY4741 but P_{GAL1}-*3HA-TOP1* (KanMx6)], YAEH275 [BY4741 but P_{GAL1}-*3HA-TOP1* (KanMx6) *rnh201Δ* (NatMx6) *rnh1Δ* (HphMx6)], YAEH267 [BY4741 but *top1Δ* (HphMx6) pGAL1], and YAEH269 [BY4741 but *top1Δ* (HphMx6) pGAL1-*RNH201*] (23). The *TOP2* temperature-sensitive (ts) strain was HT2C1A2 (*MATa his7 ura1 top2-1ts*) (kindly provided by Dan Burke). The *TOP1 TOP2* mutant strain was W1477-5B (*MATα leu2-3,112 trp-1 can1-100 ura3-1 ade2-1 his3-11,15 top1::HIS3 top2-4ts* (kindly provided by Rodney Rothstein).

Miller chromatin spreading and EM analysis. Cells were prepared for electron microscopy (EM) analysis, mainly using method 1 as described previously (57). Briefly, yeast strains were grown at 30°C in yeast extract-peptone-dextrose (YPD) for 5 to 6 h before being diluted ~1:100 into YPD plus 1 M sorbitol and grown to mid-log phase (A_{600} = 0.3 to 0.5). Samples (1 ml) of the cell culture were transferred to prewarmed (30°C) tubes containing 5 mg of zymolyase (20T; U.S. Biological), rapidly mixed, and shaken at 30°C for 4 min. Samples were centrifuged at maximum speed in a tabletop microcentrifuge for 10 s. The supernatant fluid was withdrawn, the pellet was resuspended in 1 ml of 0.025% Triton X-100 (pH 9), and the resuspended cells were pipetted into an additional 3-ml volume of the Triton X-100 solution to ensure hypotonic lysis of the cells. Cellular contents were allowed to disperse at room temperature for 20 to 60 min

before a 1/10 volume of 0.1 M sucrose 10% formalin solution (pH 8.7 to 8.8) was added. Aliquots (~70 μl) were centrifuged onto carbon-coated copper electron microscope grids at 9,000 rpm for 5 min in an HB-4 rotor. The grids were stained with phosphotungstic acid and uranyl acetate and viewed in a JEOL 100 CX transmission electron microscope. For some experiments (e.g., see Fig. 4A), method 2 chromatin spreading conditions were used (57), which includes adding 11 mM KCl to the lysis buffer.

For *in vivo* fixation prior to EM visualization, formaldehyde (Sigma; 37% [wt/wt]) was added to yeast cultures at a concentration of 1% for 6 min prior to cell lysis for chromatin spreading. When used, mycophenolic acid (MPA; Sigma) was added to yeast cultures at a concentration of 50 μg/ml for 1 h prior to cell lysis. When used, nocodazole (Sigma) was added to yeast cultures at a concentration of 20 μg/ml for 2 to 4 h prior to cell lysis.

For analysis of polymerase density or topo-bubble frequency in gene populations, all examples of active rRNA gene regions seen on multiple EM grids from at least two separate experiments were photographed, mapped, and included in the compilation. For measurement of bubble frequency, all active rRNA genes that exhibited a polymerase-free gap in which a bubble might occur were included, corresponding to the great majority of dispersed active genes. Gene and topo-bubble lengths were measured by using ImageJ software (rsbweb.nih.gov/ij/).

ChIP. Chromatin immunoprecipitation (ChIPs) were performed as previously described (19). Exponentially growing cells (optical density at 600 nm [OD600] of ~1.0) in 100 ml of YPD medium were cross-linked with 1% formaldehyde for 20 min and then washed twice with 10 ml of cold TBS (300 mM NaCl, 40 mM Tris-HCl [pH 7.5]). The cell pellets were resuspended in 0.6 ml of FA-lysis 140 buffer (50 mM HEPES, 140 mM NaCl, 1.0% Triton X-100, 1 mM EDTA, 0.1% sodium deoxycholate) containing protease inhibitors and then disrupted in a FastPrep FP120 machine (Bio 101/ThermoSavant) at 4°C (shaking 7x for 45 s each time with 1 min on ice in between shakings). The cell extracts were collected into microfuge tubes, sonicated with eight 10-s pulses (30% output, 90% duty cycle) on ice, and then centrifuged at 14,000 rpm in an Eppendorf microcentrifuge for 5 min at 4°C. The supernatants were transferred to a new microfuge tube, and the protein content was quantified by using a Bradford assay (Bio-Rad). For immunoprecipitations (IPs), equal protein content (1.25 to 1.5 mg) per extract was incubated in 0.6-ml microfuge tubes with FA-lysis 140 solution in a total volume of 400 μl. For the input chromatin controls, 1/10 of the extract volume used for IP was processed independently without antibody addition. An anti-protein A antibody was added to the IP samples (Sigma; 1:50,000 dilution), and the tubes were rotated overnight at 4°C. One-tenth of the chromatin extract volume used for IP was used as the input control extract. The IP supernatants were added to new 0.6-ml microfuge tubes containing 60 μl of protein A-Sepharose beads (50% slurry in FA-140 buffer) and rotated at 4°C for 4 h. Beads were then washed four times with 0.5 ml of FA-lysis 140 buffer, four times with 0.5 ml of FA-lysis 500 buffer (50 mM HEPES, 500 mM NaCl, 1.0% Triton X-100, 1.0 mM EDTA, 0.1% sodium deoxycholate), and four times with 0.5 ml of LiCl detergent wash buffer (10 mM Tris-HCl [pH 8], 250 mM LiCl, 0.5% NP-40, 0.5% sodium deoxycholate, 1 mM EDTA). The immunoprecipitated material was eluted twice with 75 μl of elution buffer (5× TE + 1% sodium dodecyl sulfate) and then incubated overnight at 65°C to reverse the cross-links. DNA was purified by using a PCR purification kit (Qiagen). PCR conditions were as follows: 92°C for 3 min (1 cycle); 92°C for 30 s, 52°C for 30 s, and 72°C for 45 s (22 cycles for rDNA or 29 cycles for *ACT1*); and 72°C for 5 min (1 cycle). Reactions were run on a 1.5% agarose gel and stained with ethidium bromide. The band intensities were quantified by using ImageQuant software (Molecular Dynamics) and used to determine IP/input ratios for each primer in both cell types. IP/input ratios were normalized to the rDNA5 primer signal within each data set. The average of normalized values from three independent experiments was calculated with the standard errors.

The ChIP primers were as follows. Primer sets were as follows: rDNA1 (nucleotide [nt] positions 3 to 213 relative to +1 for the rRNA transcript), 5′ (5′-GCGAAAGCAGTTGAAGACAAGTTCG-3′) and 3′ (5′-CACACTCTGG GAATTTCTTCCC-3′); rDNA2 (positions 1061 to 1274), 5′ (5′-CGGGGAAT AAGGGGTTCGATTCCGG-3′) and 3′ (5′-CGGCTGCTGGCACCAGACTTG CCC-3′); rDNA3 (positions 2051 to 2250), 5′ (5′-GGTGCTAGCATTTGCTG GTTATCC-3′) and 3′ (5′-GCTCTATCCCCAGCACGACGGAG-3′); rDNA4 (positions 3001 to 3214), 5′ (5′-GCCTGTTTGAGCGTCATTTCCTTC-3′) and 3′ (5′-CGATAACGTTCCAATACGCTCAG-3′); rDNA5 (positions 3867 to 4074), 5′ (5′-GGCATAATGGTTATATGCCCGCCG-3′) and 3′ (5′-GCATAG TTCACCATCTTTCGGGTC-3′); rDNA6 (positions 5007 to 5224), 5′ (5′-CAG CACCTTTGCTGGCTCCGGTGC-3′) and 3′ (5′-CTGACCAAGGCCCTCAC TACCCG-3′); rDNA7 (positions 5851 to 6045), 5′ (5′-CAGGTGGGGAGTTT GGCTGGGGGCG-3′) and 3′ (5′-CCTCTAGCCTCAAATTCCGAGGG-3′);
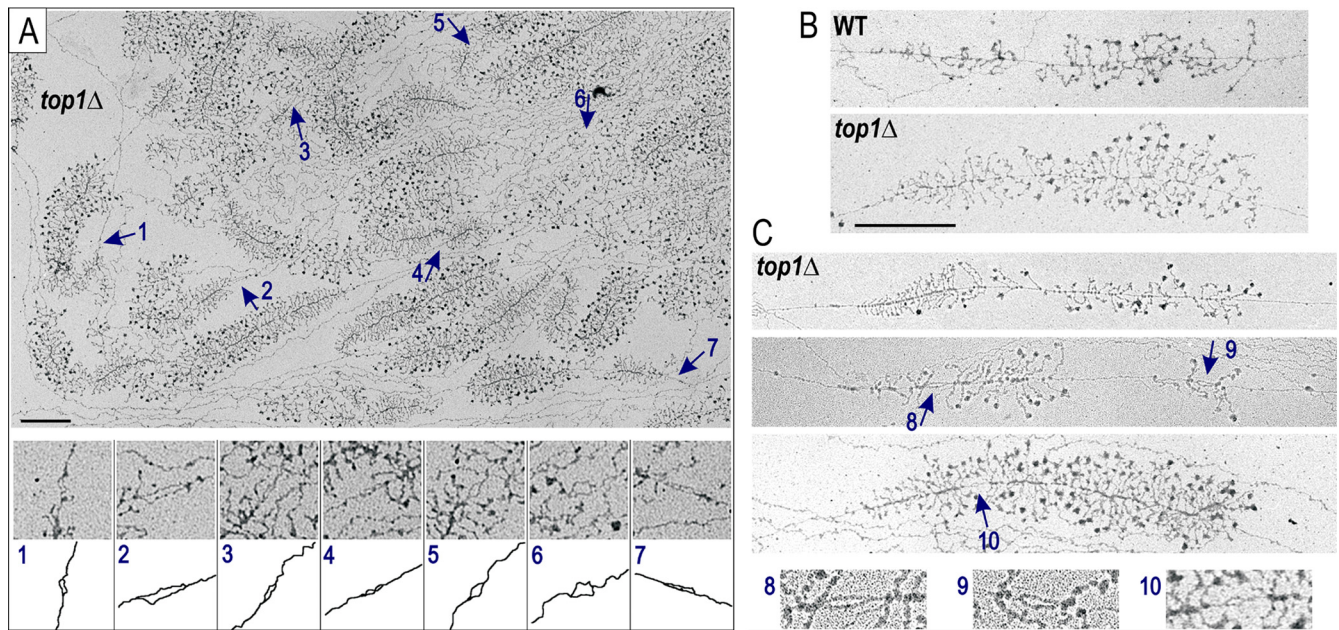
FIG. 1. rRNA genes in *top1Δ* cells are robustly transcribed and display unusual bubble structures in the active rDNA template. (A) The top panel shows an EM image of ~20 active rRNA genes from a single yeast nucleolus from *top1Δ* cells (bar, 0.5 μm). Numbered arrows point to bubble structures in genes. Bottom panel shows each bubble at a higher magnification with an accompanying trace of the DNA strand in which the bubble occurs. (B) Representative rRNA genes from the WT and *top1Δ* (SY84) strains, with each gene displaying ~average polymerase density for the strain. Bars (for genes in panels B and C), 0.5 μm. (C) Single rRNA genes from *top1Δ* cells. The genes in the two panels on top have fewer polymerases than average, with topo-bubbles in some but not all of the polymerase-free gaps (middle gene). The lower gene has high pol density with a small bubble in a small polymerase-free gap. Bubbles 8 to 10 are enlarged at bottom.

rDNA8 (positions 6607 to 6825), 5′ (5′-GTTACGATCTGCTGAGATTAAGC C-3′) and 3′ (5′-GGTACACTCTTACACACTATCATCC-3′); NTS1 (positions −2189 to −1912), 5′ (5′-GAAAGGATTTGCCCGGACAGTTTG-3′) and 3′ (5′-CTTCTTCCCAGTAGCCTGTTCCTT-3′); NTS2 (positions −265 to −26), 5′ (5′-GTATGTTTTGTATGTTCCCGCGCG-3′) and 3′ (5′-CATGAAGTAC CTCCCAACTACTTTTCCTC-3′); and ACT1, 5′ (5′-CCAATTGCTCGAGAG ATTTC-3′) and 3′ (5′-CATGATACCTTGGTGTCTTG-3′).

RESULTS

Unusual appearance of rRNA genes in *top1Δ* cells. EM visualization of nucleolar chromatin dispersed by Miller spreading allows quantitative analysis of many rRNA genes from multiple nucleoli (25, 57), thus combining the advantages of studying both individual genes and gene populations. The method was used to analyze rDNA from control yeast strains and strains lacking Top1 (*top1Δ*). These genes were robustly transcribed in *top1Δ* cells (Fig. 1A), as expected given the near-normal growth rate of *top1Δ*. In a companion study, we found that rRNA genes from *top1Δ* had, on average, somewhat more polymerases per gene compared to the control strain (examples in Fig. 1B) and more polymerase pileups than the control strain (23). In the present study we focus on the unusual bubble structures seen within the template rDNA in a subset of rRNA genes in *top1Δ*. These bubbles occurred in some but not all polymerase-free gaps in active genes and appeared to be regions of DNA strand separation. Inspection of the genes in Fig. 1A revealed 7 examples of such bubbles (arrows 1 to 7) in seven different genes from this field of ~20 active genes. Additional examples are shown in Fig. 1C (arrows 8 to 10), as are enlarged views of bubbles. Such bubbles oc-

curred in up to 30% of active genes from *top1Δ* cells. The bubbles were seen in rRNA genes from four Top1-deficient strains (Table 1) but were not seen in Top2-deficient cells (below) and have not been seen in our previous EM analyses of many different yeast strains. We call these structures "topo-bubbles."

Topo-bubbles in rDNA in *top1Δ* cells are not replication bubbles. Newly initiated DNA replication events also appear as bubbles; we sought to determine whether these could be distinguished from topo-bubbles in the rDNA. There is an origin of replication in each nontranscribed spacer (NTS) in all ~150 rDNA repeats (r-ARS in Fig. 2A); ~20% of these fire during each S phase (45). Replication bubbles seen shortly after firing occurred at the expected position in the NTS (63), shown in the upper EM image in Fig. 2A from *top1Δ* cells. For comparison, a topo-bubble in the 5′ region of an rRNA gene is shown in the lower EM image in Fig. 2A (enlarged image in inset). A set of neighboring replication and topo-bubbles is shown (Fig. 2B), as are examples of longer replication and topo-bubbles (Fig. 2C). The two types of bubbles differed by several criteria. First, replication bubbles typically had a particle at each end, corresponding to the replication machinery, whereas topo-bubbles were only rarely bracketed by particles, which could be identified as RNA polymerases (see below). Second, topo-bubbles were within the active genes, whereas short replication bubbles originated in the NTS. Third, replication bubbles ranged widely in length, from very small to 8 to 9 μm, corresponding to 27 to 30 kb or ~3 rDNA repeats (Fig. 2D). Topo-bubbles were on average much shorter, 0.12 μm or

TABLE 1. Topo-bubble length in different *top1Δ* yeast strains

Strain	Topo-bubble length[a]			No. of bubbles
	Avg (μm)	SD	Range (μm)	
Combined *top1Δ* strains	0.123 (~415 bp)	0.080	0.023–0.635 (~77–2,140 bp)	220
Individual *top1Δ* strains				
SY84 (*top1Δ*)	0.113	0.075	0.035–0.635	84
W1854-2A (*top1Δ*)	0.140	0.100	0.024–0.498	71
YB168 (*top1Δ Tap-RFA1*)	0.119	0.070	0.047–0.373	20
YAEH267 (*top1Δ*)	0.119	0.054	0.042–0.271	45
W1477-5B (*top1Δ top2-ts*)				
23°C	0.112	0.064	0.023–0.378	106
35°C	NA	NA	NA	0

[a] Ranges in parentheses were derived by assuming an average DNA compaction of 3,370 bp per 1 μm of rRNA gene length in EM spreads, which was determined empirically from rRNA genes measured for this study. This is somewhat compacted from B-form DNA (2,940 bp/μm). NA, not applicable because no topo-bubbles were seen in rRNA genes in this strain after inactivation of Top2 at 35°C for 2 to 4 h.

~420 nt, with the largest seen being ~2.1 kb (Fig. 2D and Table 1). Lastly, multiple topo-bubbles (two to four) occurred in 27% of bubble-containing rRNA genes, whereas only a single replication origin is present per repeat. We conclude that the DNA bubbles seen in active genes in *top1Δ* strains are not replication intermediates.

Topo-bubbles are not R-loops, but their appearance is dependent on RNase H activity. Since R-loops might appear as bubbles in transcribed DNA (32), we addressed the relationship of topo-bubbles to transcriptional R-loops. R-loops are increased in DNA that is under negative torsional stress, including rRNA genes in *E. coli topA* mutants (21, 50) or in yeast cells lacking both Top1 and RNase H (23). RNase H removes R-loops by digesting the RNA strand of RNA-DNA hybrids

(16). If topo-bubbles are R-loops, we anticipated that they would be stabilized when RNase H is inhibited in Top1-depleted strains, leading to increased numbers and/or length of bubbles, and removed when RNase H is overexpressed. This was found not to be the case.

To decrease RNase H activity, it was necessary to inhibit the expression of both RNase H1 and RNase H2, which have overlapping functions (1). In *rnh1Δ rnh201Δ* double-mutant strains, RNase H activity is decreased to a small percentage of normal (1, 23). Growth and rRNA synthesis are not clearly affected, but the combined mutation is synthetic lethal with *top1Δ* (23). We analyzed rRNA genes in P_{GAL}-*TOP1 rnh1Δ rnh201Δ* strains following depletion of Top1 by transfer from galactose to glucose medium for 6 h. This is 4 h prior to
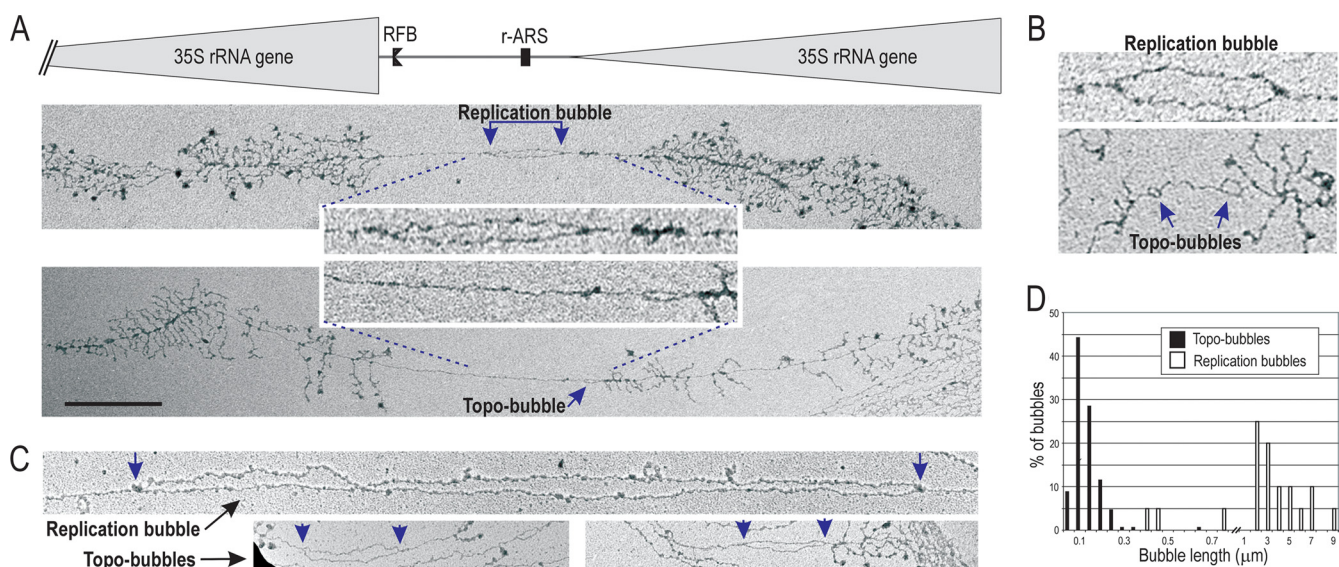

FIG. 2. Topo-bubbles can be distinguished from replication bubbles. (A) Schematic of the tandem rDNA repeat showing position of the origin of replication (r-ARS) and replication fork barrier (RFB) in the nontranscribed spacer (NTS). Shown below this, and aligned in terms of gene-spacer-gene position, are rDNA regions from *top1Δ* cells displaying either a replication bubble in the NTS (bracketed arrows) or a topo-bubble within and near the 5' end of the 35S rRNA gene (arrow). Bubbles are enlarged in inset. Bar, 0.5 μm. (B) Examples of replication and topo-bubbles from nearby regions on an EM grid. (C) Examples of longer bubbles of both types. Vertical arrows indicate bubble ends. Replication bubble (top) is ~10 kb long. Topo-bubbles (bottom) are ~1.7 and ~1.35 kb. (D) Plot of bubble length distribution for 147 topo-bubbles and 20 replication bubbles, from SY84 and W1854-2A *top1Δ* strains.
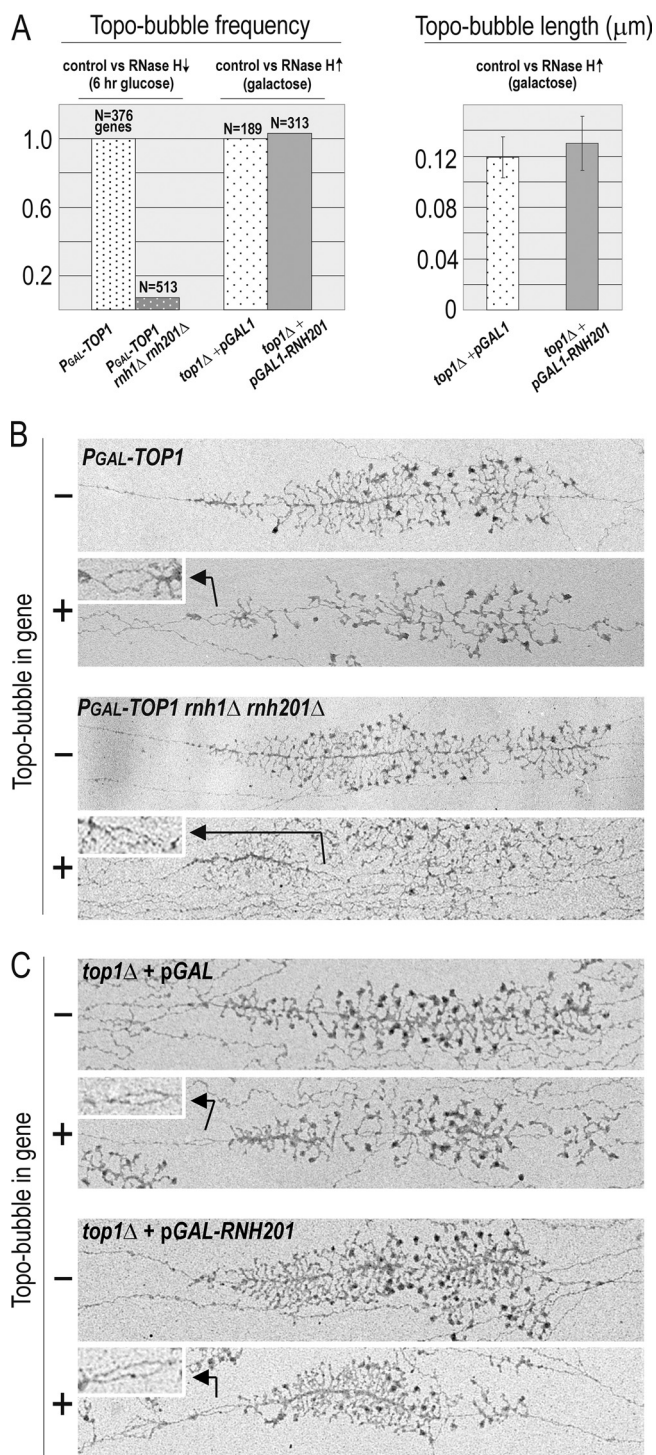
FIG. 3. Effect of RNase H under- and overexpression on topo-bubbles in Top1-deficient cells. (A) The left plot shows the topo-bubble frequency in Top1-deficient cells in conditions of RNase H under- and overexpression. For RNase H underexpression, strain YAEH275 (P_{GAL}-TOP1 rnh1Δ rnh201Δ) was switched from galactose to glucose medium for 6 h to deplete Top1. Its control strain was YAEH271 (P_{GAL}-TOP1), which was also depleted of Top1 for 6 h. For RNase H overexpression, strain YAEH269 (top1Δ+pGAL-RNH201) was grown in galactose medium for expression of RNH201. Its control strain YAEH267 (top1Δ+pGAL) was similarly grown. Topo-bubble frequency in experimental strains (i.e., Top1-deficient and plus or minus RNase H) is shown as a fraction of the frequency in Top1-

deficient control strains; (see the text for the frequency of bubble-containing genes). The bar graph on the right shows the average topo-bubble length (error bars indicate the standard deviation) in YAEH267 compared to YAEH269 using same gene populations used for topo-bubble frequency. (B) Representative rRNA genes from RNase H underexpression experiment in panel A, showing examples with (+) and without (−) topo-bubbles from both strains. Topo-bubbles within genes are enlarged in insets (arrows). (C) Same as panel B for RNase H overexpression experiment.

manifestation of a growth defect and 8 to 10 h prior to growth inhibition (23), thus avoiding any indirect effects of poor growth rate. For comparison, *TOP1* expression was similarly repressed for 6 h in a strain expressing wild-type (WT) RNase H levels. As shown in Fig. 3A, topo-bubble frequency decreased by more than 90% in cells deficient for both RNase H and Top1 compared to cells deficient for Top1 only. Analysis of individual rRNA genes revealed 23 bubbles in 376 genes (6.1%) after 6 h depletion of Top1, whereas only 2 of 513 genes displayed bubbles (0.4%) in *rnh*Δ cells after 6 h Top1 depletion (Fig. 3A; examples in Fig. 3B). In the presence of Top1 (growth in galactose), no topo-bubbles were seen in either strain (not shown). The higher topo-bubble frequency in *top1*Δ strains (~30% of genes) compared to *GAL::TOP1* strains grown for 6 h on glucose (6% of genes) may reflect the different degrees of Top1 depletion.

We sought to determine whether topo-bubbles were reduced upon overexpression of RNase H, as might be expected for R-loops. To increase RNase H activity, RNase H2 was overexpressed by Gal-induction of *RNH201*, a treatment shown to increase digestion of telomeric R-loops in yeast (48). Western blotting confirmed the robust induction of *RNH201* by galactose in strain YAEH269, which is also *top1*Δ (23). We measured topo-bubble length and frequency in YAEH269 after growth in galactose and compared these parameters to *top1*Δ cells in the same conditions. There was no significant difference in the frequency (30 versus 31% of genes) or average length (0.12 versus 0.13 μm) of topo-bubbles in *top1*Δ cells in the presence of endogenous versus overexpressed levels of RNase H (Fig. 3A; examples in Fig. 3C).

Combined data indicate that topo-bubbles are not R-loops, since they were not stabilized when RNase H was deficient and they were not destabilized when RNase H was overexpressed. Rather, efficient formation of topo-bubbles was dependent on RNase H activity (Fig. 3A). We propose that in the absence of Top1, digestion of R-loops is needed to clear blocks to transcription elongation and thus allow the buildup of torsional stress that generates topo-bubbles (see model in Fig. 8).

Evidence that topo-bubbles are regions of DNA helix melting. Since topo-bubbles did not have characteristics of replication bubbles or R-loops, we considered that they might consist of unwound single-stranded DNA. Their appearance in EM images supported this conclusion, since both sides of the topo-bubbles had a similar form, which is expected of single-stranded DNA bubbles but not of R-loops. Also, there was no visible evidence of RNA involvement in the bubbles; that is, no RNA attached to a nearby polymerase could be seen feeding into them, and no free RNA tails emerged (Fig. 4A). The presumed single-stranded DNA within the topo-bubbles gen-
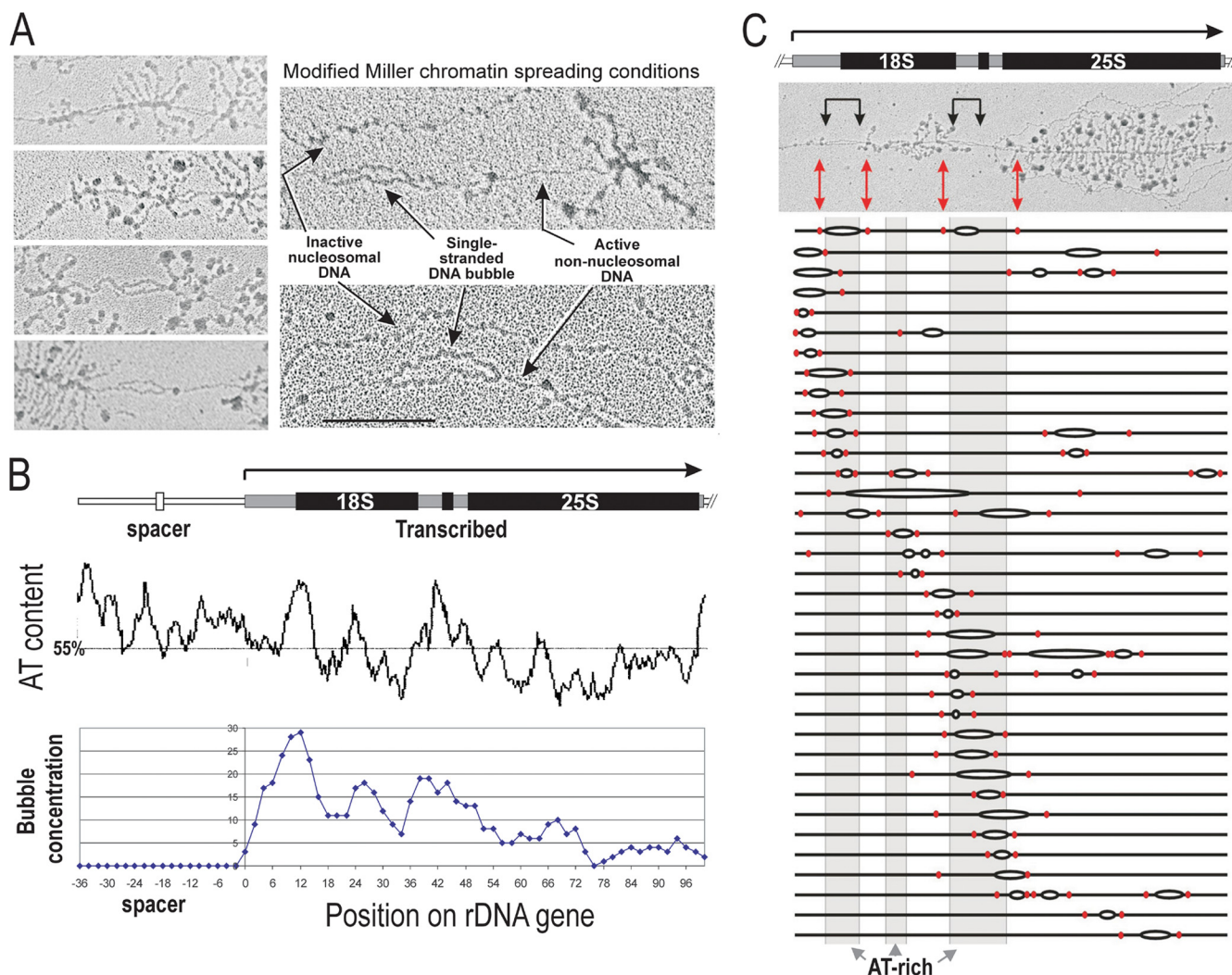
FIG. 4. Topo-bubbles appear as regions of DNA helix melting and preferentially occur in AT-rich regions of the gene. (A) Shown at left are portions of four active rRNA genes from *top1*Δ with topo-bubbles showing typical characteristics: both sides of the bubble appear similar and with no evidence of RNA involvement, even when immediately juxtaposed to RNA polymerases. At the right are portions of two active rRNA genes from *top1*Δ obtained using modified Miller spreading conditions (KCl concentration increased by 11 mM) (57). In these conditions, DNA in topo-bubbles appears thicker than flanking double-stranded DNA (see the text). Bar, 0.1 μm. (B) Schematic of rDNA repeat at top is aligned with a graph showing the percent AT content across the repeat (middle) and a plot of bubble position across the repeat (bottom). The latter was derived by normalizing gene length to 100 U, dividing each gene into 50 bins of 2 U each, and scoring each bin across the gene as positive or negative (for denatured DNA at that position) for each bubble-containing gene analyzed. *n* = 101 genes. (C) Gene schematic is aligned with EM of an active rRNA gene with two topo-bubbles (bracketed black arrows). Double-headed red arrows indicate nearest-neighbor RNA polymerases up- and downstream of both bubbles. This gene and 35 additional genes are schematized below the EM image, with each gene normalized in length and with topo-bubble occurrence shown. Nearest-neighbor polymerases up- and downstream of each bubble are shown as red ovals. Shaded bars indicate the three most AT-rich regions, as shown in panel B.

erally appeared similar to the flanking double-stranded DNA (Fig. 4A, left panel), but typical Miller-spread conditions are known to remove some nucleic-acid-bound proteins. When we used more physiological spreading conditions (56, 57), both strands of DNA within the bubble still appeared similar, but were now thicker than the flanking DNA (Fig. 4A right). Single-stranded DNA forms complexes with ssDNA binding proteins and has been shown to appear thicker than a DNA helix in EM preparations (73).

Mapping of topo-bubble positions revealed that they occurred preferentially in AT-rich regions of the rRNA gene (Fig. 4B and C). AT-rich helices have fewer hydrogen bonds

than GC-rich helices and thus are more susceptible to thermal and torsional denaturation (54). Bubble positions were mapped for 101 genes from four different *top1*Δ strains with similar results; combined data are shown in Fig. 4B, and representative genes in Fig. 4C. The three most frequently melted DNA regions mapped within the first half of the gene and overlapped substantially with the three most AT-rich regions (Fig. 4B). Although the nontranscribed spacer is AT-rich, bubbles were not seen in this region, strengthening the association between topo-bubbles and transcription-induced torsional stress. A gene with two topo-bubbles (black brackets) in AT-rich regions is shown at the top of Fig. 4C, which also shows
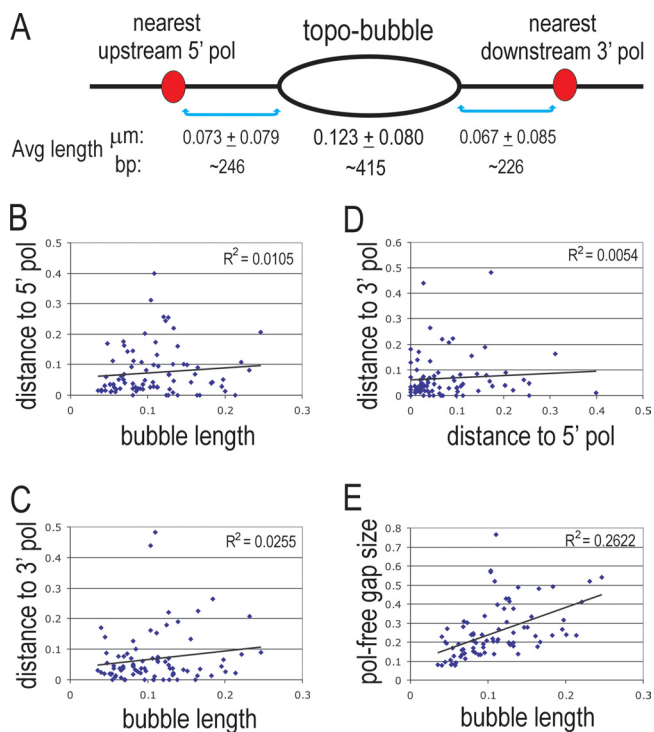
FIG. 5. Polymerases do not pile up upstream or run off downstream of topo-bubbles. (A) Schematic of analysis in which lengths were measured between bubbles ($n = 85$) and the nearest polymerases. Average lengths between nearest polymerases and nearest bubble fork are indicated in μm and approximate base pairs. Topo-bubble length ($n = 220$) from Table 1. (B and C) Relationship between bubble length and distance to nearest upstream (B) or downstream (C) polymerase. (D) Relationship between distance to nearest upstream polymerase and distance to nearest downstream polymerase. (E) Relationship between bubble length and polymerase-free gap size.

maps of the topo-bubble position within that gene and 35 additional genes (with AT-rich regions shaded gray). The nearest RNA polymerases flanking the bubbles are also shown (red arrows and dots). Topo-bubbles are typically flanked by polymerases, but the melted region is free of polymerases.

The EM appearance of topo-bubbles and their locations in AT-rich DNA are consistent with regions of DNA unwinding due to transcription-induced negative torsional stress.

Topo-bubbles do not appear to interfere with Pol I elongation. We analyzed the position of polymerases flanking topo-bubbles (Fig. 5) to determined whether topo-bubbles impair elongation, such as occurs with cotranscriptional R-loops (23, 32, 71). For example, polymerases upstream of the bubble might be closer in distance and/or denser in distribution if elongation is impaired, and polymerases downstream might be farther away and lower in density, as they run off the gene. We measured the distance of the nearest upstream polymerase to the upstream fork of the bubble and the distance of the nearest downstream polymerase to the downstream fork for 85 topo-bubbles. As diagrammed in Fig. 5A, these average distances were similar for the nearest upstream and downstream polymerases, (ca. 225 to 250 nt), with no evidence that polymerases were running up to the bubble or running off downstream of the bubble. Some of the nearest polymerases were immediately

apposed to the fork, indicating that such placement is topologically possible but is not a necessity, e.g., as a physical barrier to stop DNA unwinding. In general, there was a broad range in the distances between nearest polymerases and topo-bubbles, as shown in Fig. 5B to D. The plots show lack of correlation between bubble length and nearest polymerase distance and lack of correlation between the nearest 5′ and 3′ polymerase for a bubble. These data provide no evidence that polymerases are either blocked upstream or run off downstream of bubbles and also no evidence that neighboring polymerase position is affected by the degree of topological stress (as measured by the degree of DNA melting) and thus no evidence that elongation is affected.

Pileups of closely spaced polymerases are also indicative of slowed elongation, occurring with a certain frequency in WT strains and increasing in elongation mutants (23, 82). Visual inspection of all bubble-containing rRNA genes from the different $top1\Delta$ strains indicated that pileups were no more frequent or longer in these genes than in genes from WT cells. Furthermore, the observed pileups were not preferentially upstream of bubbles. This visual inspection was confirmed by quantitative analysis of genes from P_{GAL}-TOP1 cells after 6 h Top1 depletion (same population analyzed in Fig. 3A and B). That is, pileups of five or more polymerases were not more frequent in bubble-containing genes in Top1-depleted cells (occurring in 22% of genes) than in genes in the control strain not depleted of Top1 (occurring in 37% of genes).

In conclusion, analyses of nearest up- and downstream polymerases as well as polymerase pileups in bubble-containing genes provided no evidence that elongation was slowed by negative torsional stress sufficient to melt the template DNA.

Topo-bubbles are not seen when elongation rate is slowed in $top1\Delta$ cells. Bubble length was similar in different $top1\Delta$ strains and in a $top1\Delta$ $top2$-ts strain at permissive temperature (Table 1, Fig. 3A, and Fig. 5A). Based on correlation of the bubble position with AT-richness of the rDNA and the lack of correlation of bubble length with polymerase-free gap length (Fig. 5E), it appears that DNA base composition strongly influences the extent of template melting seen in chromatin spreads. No conditions were noted that influenced bubble length, but three conditions were found that significantly decreased bubble frequency, all of which are predicted to slow Pol I elongation: depletion of Top1 in the absence of RNase H (Fig. 3A) (23), inactivation of Top2 in the absence of Top1 (see below), and treatment of $top1\Delta$ cells with MPA, which decreases intracellular guanine nucleotide concentration, thus slowing elongation (6, 67). In the latter experiment, 1-h treatment of SY84 $top1\Delta$ cells with MPA resulted in a 8.5-fold decrease in topo-bubbles, from 10.5% of genes with topo-bubbles in untreated cells ($n = 95$) to 1.6% in treated cells ($n = 184$). In addition to slowing elongation, these three conditions also increased polymerase density on rRNA genes (23) (Fig. 7 and data not shown). The absence of topo-bubbles may be due to fewer polymerase-free gaps and/or to slowed polymerase movement such that negative torsional stress is less likely to build up. These results support our hypothesis that topo-bubbles represent the buildup of negative torsional stress in polymerase-free gaps behind elongating polymerases.

Single-stranded gene regions exist *in vivo* in rRNA genes in *top1*Δ cells. Unconstrained negative topological stress in DNA can be absorbed either by DNA unwinding or by negative supercoiling (Fig. 6A). These inter-convertible configurations have the same linking number (Lk) but differ in twist and writhe. ("Twist" refers to the number of double helical turns [one per 10.5 bp in B-form DNA], and "writhe," or supercoiling, refers to the number of times the double helix crosses over itself when projected in two dimensions [65].) Since the melted form is favored by conditions encountered in Miller chromatin spreading, i.e., by low ionic strength and by dispersing DNA into a more linear configuration, we sought to determine whether there was evidence that the single-stranded form, rather than the supercoiled form, exists *in vivo*. We reasoned that if melted DNA exists it is likely to be bound by RPA, which is the most abundant single-stranded DNA-binding protein in eukaryotic cells (34), is present in nucleoli (33), and is expected to quickly bind any ssDNA that forms in the cell (20). This was tested by ChIP analysis using TAP-tagged Rfa1 (*TAP-RFA1*), the large subunit of the RPA complex, in control and *top1*Δ strains. EM analysis confirmed topo-bubble occurrence at a typical frequency and length in this *top1*Δ strain (Table 1). As shown in Fig. 6B, *top1*Δ cells showed a reproducible increase in Rfa1 bound to transcribed regions of the rDNA compared to control cells, but no increase was seen over the rDNA spacer or the *ACT1* gene.

In another approach to determine whether topo-bubbles exist in cells, chromatin spreading was performed following *in vivo* formaldehyde fixation, as is done in standard ChIP procedures and is generally accepted to capture *in vivo* interactions (41). Although this fixation rendered chromatin much more difficult to spread, topo-bubbles could be seen in active rRNA genes in *top1*Δ cells, with two examples shown in Fig. 6C. Thus, based on the increased presence of RPA (Fig. 6B) and the visualization of topo-bubbles after *in vivo* formaldehyde fixation (Fig. 6C), we conclude that at least some of the torsional stress is absorbed by DNA denaturation *in vivo*.

When Top2 is inactivated, rRNA genes exhibit signs of positive topological stress. Full-length rRNA is not made if Top1 and Top2 activity are both absent, but there are no major rRNA synthesis defects if either is inactivated individually (11, 23, 66). We visualized rRNA genes after Top2 inactivation to compare their features to those from *top1*Δ cells. Hundreds of rRNA genes were inspected from *top2-ts* cells grown for 2 to 3 h at 35°C or for 2 to 4 h at 35°C in the presence of nocodazole to prevent completion of mitosis (29). No topo-bubbles were observed, even in genes with polymerase-free gaps. (A control experiment showed the appearance of topo-bubbles in *top1*Δ cells at 35°C [data not shown]). Instead, inactivation of Top2 resulted in increased polymerase density on active genes, a finding consistent with slowed elongation, as seen in the nucleolar overviews in Fig. 7A and B comparing genes from permissive (23°C) to Top2-inactivated cells (35°C). Although genes at both temperatures display many nascent transcripts, note the increase in Pol I density after Top2 inactivation as shown by the dense polymerase "backbones" along the rDNA at 35°C (Fig. 7B). This visual impression was confirmed by counting polymerases on >100 active rRNA genes from both permissive and restrictive temperatures (inset Fig. 7A), with results showing a 26% increase in average number of poly-
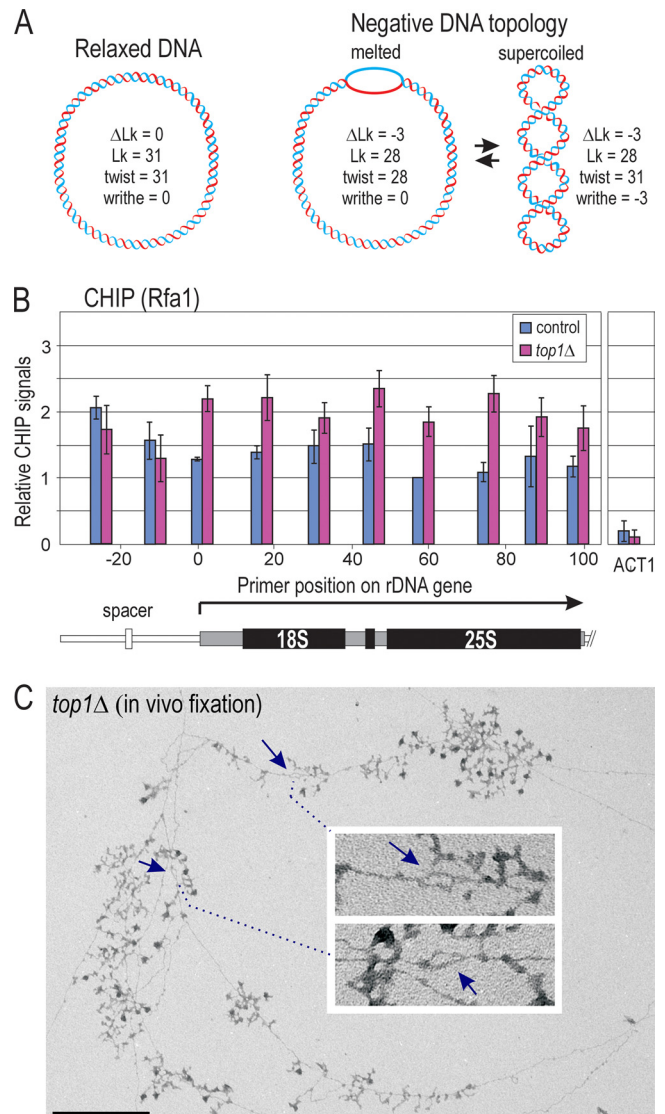

FIG. 6. Evidence that some negative topological stress occurs as melted DNA in *top1*Δ cells *in vivo*. (A) Schematic of the two inter-convertible forms of DNA under negative topological stress: melted versus negatively supercoiled. Shown is a hypothetical DNA plasmid of 325 bp, which has a relaxed linking number (Lk_0) of 31 (i.e., 325/10.5 = 31). The linking number (Lk) has contributions from twist and writhe, i.e., Lk = twist + writhe. Relaxed plasmid on left has linking number (Lk) of 31 due to 31 helical twists, and thus its $\Delta Lk = 0$, where $\Delta Lk = Lk - Lk_0$ (difference between the actual and the relaxed linking number). On the right is a plasmid of the same length but under negative topological stress ($\Delta Lk = -3$), which can be relieved by melting a portion of the DNA or by negative writhe, both of which allow maintenance of stable B-form helix in most of the DNA. (B) ChIP analysis of occupancy of single-stranded DNA-binding protein RPA large subunit (encoded by *RFA1*) over the rDNA repeat and on *ACT1* gene. Shown are the relative ChIP signals in control strain YB169 (*TAP-RFA1*) versus *top1*Δ strain YB168 (*top1*Δ, *TAP-RFA1*) after normalization to the rDNA5 primer within the rRNA gene. Error bars show standard error of the mean for three independent experiments. (C) EM images of several rRNA genes using modified Miller spreading conditions in which formaldehyde is added to cells prior to cell disruption, mimicking conditions used for ChIP fixation. Arrows indicate topo-bubbles in two nearby genes. Bubbles shown enlarged in the inset. Bar, 0.5 μm.
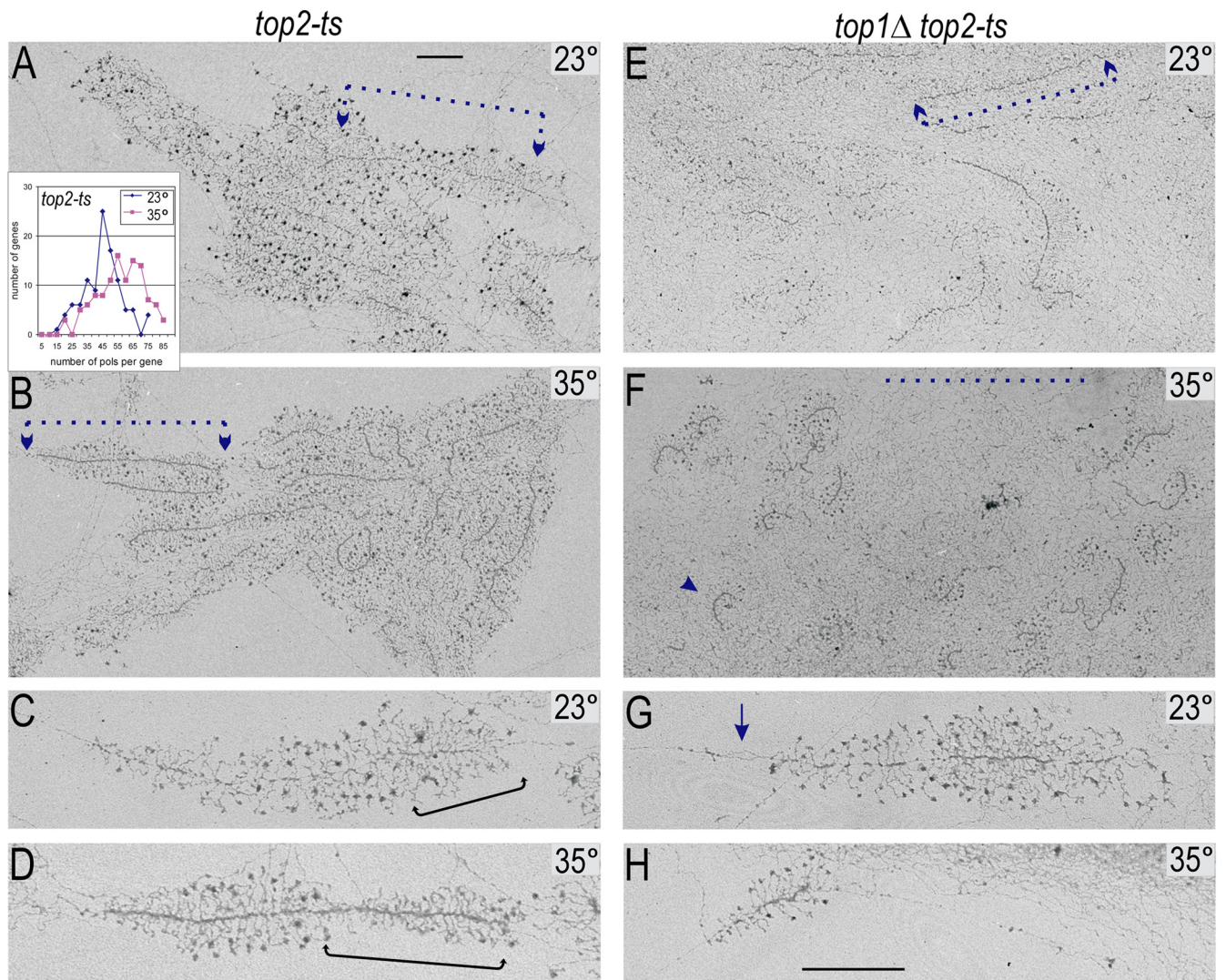
top2-ts

top1Δ top2-ts

FIG. 7. Top2 inactivation results in slow elongation in rRNA genes. (A to D) Representative rRNA genes from *top2-ts* cells at permissive (23°C) and restrictive (35°C for 2 h) temperatures, as labeled. The inset in panel A shows a polymerase density plot comparing polymerases per gene in *top2-ts* (strain HT2C1A2) at 23°C versus 35°C for 2 h. On average, there were 45 polymerases/gene at 23°C ($n = 105$ genes) and 57 polymerases/gene at 35°C ($n = 113$). The difference between these mean values is significant, with a *t* test *P* value of 2.6×10^{-9}. (E to H) Representative rRNA genes from *top1Δ top2-ts* cells at permissive (23°C) and restrictive temperatures (35°C for 2 h), as labeled. Panels A, B, E and F are at the same magnification and show overviews of nucleolar regions, including multiple rRNA genes for each condition (bar, 0.5 μm). Dotted-line brackets in panels A, B, and E (all the same length, equal to that of an active rRNA gene) are aligned with single rRNA genes, each of which is transcribed from 5′ to 3′ end. The same length dotted line is shown in panel F but is not aligned with a gene because in these conditions (Top1 and Top2 depletion) no genes are seen that are transcribed for this length. Instead, individual active genes appear as relatively short regions with very dense polymerase backbones (example, arrowhead in panel F), suggesting that polymerases are unable to traverse the entire gene. Panels C, D, G, and H (at same magnification) show single active rRNA genes for each condition (bar, 0.5 μm). Brackets in panels C and D indicate regions of the gene in which most of the transcripts have been cleaved in an early rRNA processing step (see the text). (The gene in panel D is the same as the bracketed gene in panel B. For improved clarity, Photoshop was used to remove a nearby gene seen in panel B from the image in panel D.) An arrow in panel G indicates a topo-bubble. The gene in panel H is not fully transcribed, as shown by the length of its transcribed region in comparison to fully transcribed genes in panels C, D, and G. This is attributed to poor processivity (see the text).

merases/gene after Top2 inactivation (see the legend for details; $P = 2.6 \times 10^{-9}$).

A second characteristic indicator of slowed elongation was seen in ~15% of rRNA genes as Top2 was inactivated, i.e., a "double gradient" of transcript length, as seen in the gene in Fig. 7D. We previously showed that pre-rRNA cleavage at site A2 to separate small and large subunit pre-rRNAs typically occurs on nascent transcripts at about the time that Pol I reaches the latter third of the gene (37, 56). In WT rRNA genes, this manifests as a series of transcripts in the latter portion of the gene that are shorter than expected and are missing the large 5′-terminal knobs (see Fig. 7C, bracketed transcripts). When elongation was slowed as Top2 was inactivated, A2 cleavage plus subsequent processing events proceeded efficiently, while the polymerases dawdled, resulting in a very obvious double gradient of transcript length (Fig. 7D).
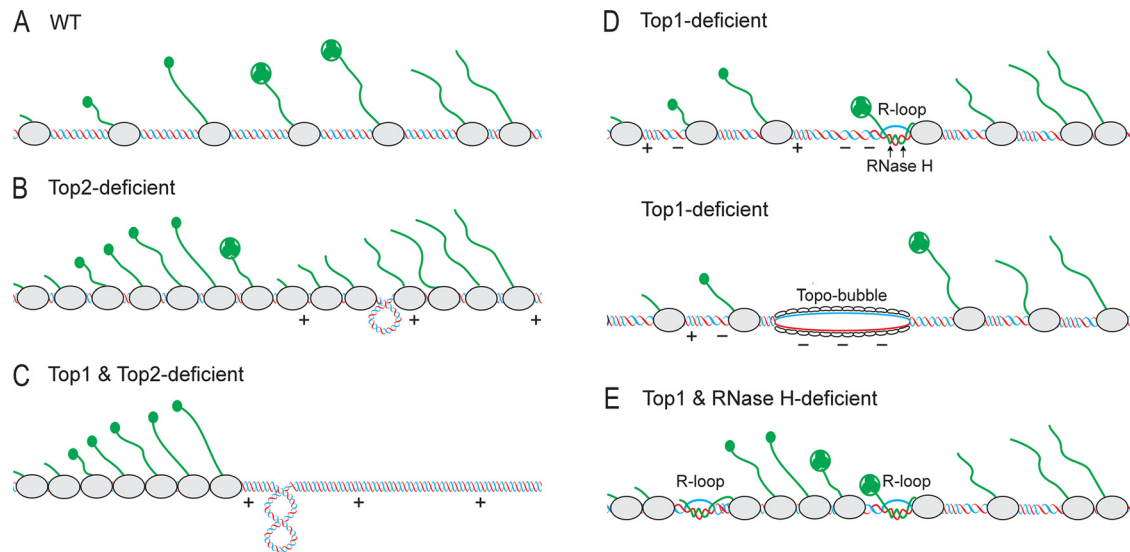
FIG. 8. Model for the effects of Top1 and Top2 depletion on Pol I transcription. (A) In WT cells, Top1 and Top2 maintain the rDNA template in a relatively relaxed topological form, as shown by the relaxed DNA between polymerases. WT rRNA genes exhibit a characteristic rRNA processing pattern, consisting of compaction of pre-small subunit RNA into a large 5′-terminal knob (SSU processome), followed by cotranscriptional cleavage to separate small subunit pre-rRNA (released and no longer visible in chromatin spreads) from large subunit pre-RNA (still extruding from the polymerase) (37, 56). (B) In cells deficient in Top2 activity, polymerases are tightly packed on most rRNA genes, and cotranscriptional cleavage is often "advanced" (double-gradient pattern) due to continued processing on dawdling polymerases. Both of these features are characteristic of slow elongation, which is consistent with increased positive torsion ("+" signs) and/or supercoiling in the absence of Top2. Although DNA writhing is not seen in EM spreads, its *in vivo* presence is inferred (as shown by the positive supercoil) since writhed DNA is the substrate for Top2 (61). (C) In cells deficient for both Top1 and Top2 activity, polymerases are rarely seen to transcribe beyond the first half of the gene, which is consistent with DNA so tightly wound ("+" signs and positive writhe) that it resists the unwinding necessary for transcription (23, 66). (D) In Top1-deficient cells, many genes show no evidence of topological abnormalities, presumably due to the action of Top2 and to local dissipation of transcription-induced positive and negative stress between elongating polymerases ("+" and "−" signs between polymerases). Excess negative torsion (due to more widely spaced polymerases) results in DNA breathing which favors the formation of R-loops (the top gene in panel D). Such R-loops are transient due to endogenous RNase H activity (see reference 23 and results in the present study). In many genes (e.g., the bottom gene in panel D), sufficient negative torsion accumulates to melt the template DNA, particularly in AT-rich regions. Evidence suggests that the melted DNA is bound by RPA (peanut shapes on bubble). (E) When RNase H activity is compromised in Top1-deficient cells (P_{GAL}-TOP1 rnh1Δ rnh201Δ), topo-bubble formation greatly decreases (Fig. 3), and transcript density increases (23). We propose that undigested R-loops significantly slow Pol I elongation, disallowing the accumulation of hypernegative topological stress and the formation of topo-bubbles.

This double-gradient pattern, which is also sometimes seen after depletion of Top1 in rnhΔ strains (Fig. 3B, third gene down), was not seen on bubble-containing genes from top1Δ strains, adding to the evidence that elongation was not slowed by topo-bubbles, as argued above. The simplest explanation for slowed elongation when Top2 is inactivated is increased positive topological stress impeding the forward movement of Pol I.

We next examined rRNA genes in top1Δ top2-ts cells at both permissive and restrictive temperatures (Fig. 7E to H). At permissive temperature (23°C), rRNA genes resembled those from top1Δ cells (Fig. 7E), including many genes with topo-bubbles (e.g., Fig. 7G), as expected due to the absence of Top1. However, at 35°C in the double mutant no bubbles were visible, but a severe processivity defect was observed (Fig. 7F and H). Polymerases and attached transcripts were densely packed toward the 5′ half of the gene and were generally absent at the 3′ end of the gene. That is, rRNA genes had recognizable 5′ ends but were shorter than expected in length (Fig. 7F and H), a finding consistent with the inability of polymerases to elongate to the end of the genes due to extreme positive topological stress in front of the leading polymerase. When both Top1 and Top2 activity are very deficient, many rRNA genes are excised as extrachromosomal rings (36). Although our EM analysis has

focused on chromosomal rRNA genes, biochemical evidence indicates a general failure in Pol I processivity in these conditions (23, 66).

These EM results show that inactivation of Top2 results in slowed elongation, a finding consistent with a net increase in positive supercoiling in active rRNA genes. The severe processivity defect seen when both Top1 and Top2 activity are deficient confirms and extends this result seen previously using biochemical methods (23, 66) and demonstrates that results obtained by EM analysis are consistent with results obtained with more standard approaches.

DISCUSSION

This report represents the first gene visualization approach to study the *in vivo* effects of topoisomerase depletion on transcription, focusing on the rRNA gene in its normal chromosomal context, thus bypassing problems that arise when studying genes on circular plasmids (27, 66, 69, 80). The results are summarized in the model in Fig. 8. In comparison to the WT (Fig. 8A), many rRNA genes in cells deficient in Top2 activity (Fig. 8B) exhibited two indicators of slowed elongation rate: higher polymerase density and an advanced (double-gradient) rRNA processing pattern. These results suggest a net

increase in positive torsion in active genes in cells lacking Top2 activity (Fig. 8B). In cells deficient for both Top1 and Top2 activity (Fig. 8C), polymerases were rarely seen to progress beyond the first half of the gene, which is consistent with DNA so tightly wound as to resist the unwinding necessary for transcription (23, 66). Although DNA writhing is not seen in our chromatin spreads, its *in vivo* presence is inferred when Top2 activity is deficient (Fig. 8B and C) since writhed DNA is the Top2 substrate (61, 65).

In cells deficient for Top1 (Fig. 8D) many active genes accumulated high levels of negative torsional stress, which was dependent on RNase H activity (top gene) and appeared as melted DNA (bottom gene). The combined absence of Top1 and RNase H (Fig. 8E) greatly decreased topo-bubble formation (Fig. 3A) while increasing Pol I pausing and DNA:RNA hybrid occupancy on the gene (23). These results indicate a role for RNase H in accumulation of hypernegative topological stress, which we attribute to its role in digesting R-loops, allowing continued transcription. Although we did not see any convincing R-loops in the presence or absence of RNase H (perhaps because they may be considerably shorter than topo-bubbles and/or less amenable to visualization by our EM approach), there is suggestive evidence to include them in our model. Thus, a transient R-loop is shown in a region where DNA is beginning to unwind (Fig. 8D), and undigested R-loops are shown impeding transcription when both Top1 and RNase H are deficient (Fig. 8E).

Does negative topological stress exist as melted DNA *in vivo*? In highly transcribed genes, the negative torsion generated behind one polymerase may be cancelled by the positive torsion generated ahead of the next one, lessening the need for topoisomerase activity (Fig. 8A and D) (46, 76). However, this canceling effect is lost if a polymerase is not followed closely by another polymerase, allowing negative torsional stress to accumulate in the resulting polymerase-free gap. Such stress can be absorbed either by partial DNA melting or by increased negative writhe (Fig. 6A), both of which allow most of the DNA to maintain a relatively constant twist near 10.5 bp/turn, which is preferred due to the stability conferred by base-pairing and stacking (8, 60, 65). Our observations of DNA bubbles in active genes after *in vivo* cross-linking (Fig. 6C), together with the increased presence of the ssDNA binding protein RPA in the gene (Fig. 6B), suggest that DNA melting absorbs at least some of the negative stress in cells. Additional indirect evidence for the existence of topo-bubbles is that they are not relaxed by Top2, which would be able to resolve the crossovers in negatively writhed DNA, but would not recognize underwound DNA. The greatly enhanced psoralen accessibility of rDNA observed in *top1*Δ cells but not in Top2-deficient cells (15) also points to a loosened rather than a supercoiled structure in the former but not the latter, in agreement with our results.

Dynamic breathing in torsionally stressed DNA, which is more likely to occur in AT-rich regions, would provide an opportunity for RPA to bind. Such binding is energetically favorable because it relaxes negative torsional stress and is self-limiting, proceeding until the driving stress is removed (20, 54). RPA needs only a short (8- to 10-nt) region of ssDNA to initiate binding and *in vitro* studies have shown RPA-induced

unwinding at AT-rich regions on plasmids under negative torsional stress (73), similar to the scenario we propose here.

Relationship of topo-bubbles to RNase H activity and R-loops. One explanation for the dependency of topo-bubble formation on RNase H activity is that elongation is slowed in its absence (due to unresolved R-loops) such that sufficient negative stress does not accumulate (Fig. 8E). It is also possible that transient R-loop formation plays a more direct role in DNA melting, e.g., the strand separation that occurs in R-loop formation might provide the entry point for RPA binding and topo-bubble formation rather than, or in addition to, dynamic breathing in the DNA as proposed above.

Extensive studies in *E. coli* have examined the interplay between topoisomerase activity, negative torsion, and R-loop formation (21). Although results in *E. coli* and yeast are not directly comparable due to differences in topoisomerase specialization (such as no gyrase counterpart in eukaryotes) and differences in the ability of endogenous RNase H to efficiently digest R-loops (2, 31), the results agree that transcription-induced negative torsion leads to R-loop formation, which contributes to elongation pauses and aberrant cleavage of nascent RNA (3, 23). It appears that *S. cerevisiae* is more efficient than *E. coli* in digesting R-loops (consistent with the more highly processive nature of eukaryotic RNase H [16]), thus allowing continued transcription and viability in *top1*Δ strains but leading to significant negative torsional stress in active genes.

Quantifying negative superhelical density. In previous studies, transcription-induced negative torsional stress has been found to dissipate upstream of active promoters and may play a role in activating transcription or replication at a nearby origin (42, 72, 80). Although we cannot rule out that this happens for a short distance upstream of the rDNA promoter or that it happens but does not melt the template, we found that topo-bubbles were not seen to extend beyond the limits of the transcribed gene even though the nontranscribed spacer is quite AT-rich (Fig. 4B). This finding is consistent with the lack of correlation between active transcription of rRNA genes and firing of the adjacent upstream replication origin (52). DNA-binding proteins and chromatin structures can form barriers that impede diffusion of torsional stress and thus increase localized supercoiling (43, 64). The promoter-bound UAF complex, which includes histones H3 and H4 and is essential for Pol I transcription and rDNA silencing, is a strong candidate for blocking such dissipation (55).

In estimating superhelical density in affected rRNA genes, we used the 6,740-bp gene as the unit in which stress can dissipate for reasons just discussed. This length of DNA will have a relaxed linking number (Lk_0) of 642 (6,740/10.5). An inactive rRNA gene will have constrained negative supercoiling due to nucleosomal packaging, but the linking number will decrease upon activation and loss of nucleosomes (51), which constrain ~1 negative supercoil each (59). Assuming ~41 nucleosomes per gene (6,740 bp/~165 bp/nucleosome = ~41), this corresponds to a ΔLk of −41 and a superhelical density (σ, where $\sigma = \Delta Lk/Lk_0$) of −0.06 for a nucleosome-free rRNA gene in control strains. The average topo-bubble was 415 bp long, corresponding to loss of ~40 twists of the DNA helix. Thus, ΔLk increases to −81 (−41 + −40) and $\sigma = −0.13$ in the average bubble-containing gene from *top1*Δ cells, about

twice the normal value. By similar calculations, genes with higher levels of melting (up to 2 kb or 30% of the gene length) due to either single large bubbles or, more frequently, to multiple smaller bubbles, have $\sigma = -0.37$, or 6 times the normal value. For comparison, the AT-rich FUSE element in the human *MYC* promoter melts when σ reaches -0.07 (40). Transcription-induced negative superhelical density in *top1Δ* cells has been reported to be more than twice the normal value (12), with more precise determination limited by the chloroquine gel method used to count topoisomers.

Transcription in genes with high negative torsion. Although unconstrained negative supercoiling has been detected in the rDNA of normal cells (47), it was somewhat surprising that genes with such high levels of negative σ continued transcribing and that *top1Δ* cells grew quite well even when 30% of rRNA genes displayed template melting. For example, hypernegative supercoiling causes growth inhibition in *E. coli* (21), and although transcription initiation increases as $-\sigma$ increases, this is true only to a certain point ($\sigma \sim -0.07$), after which it decreases (58). We presented evidence that transcription elongation was not slowed in genes with topo-bubbles. We also observed that polymerases were not seen within topo-bubbles, indicating that Pol I does not transcribe the single-stranded template. Thus, hypernegative topological stress (either as negatively writhed or melted DNA) forms no barrier to polymerase elongation, indicating that any denatured DNA reanneals as it enters the polymerase. This helical reformation would be driven by the powerful force of multiple RNAPs (4, 24) and by transcription-induced positive torsion in DNA entering the polymerase, which would cancel the negative torsion and facilitate reannealing and removal of RPA (20). Thus, as transcription continues, the melted DNA might be transiently reannealed—only to reappear as the polymerase moves down the gene. The preferential occurrence of bubbles in AT-rich regions supports their transient existence, and their dynamic appearance probably requires contributions from polymerase positions, negative torsion, and base composition of the template. In molecular simulations, denaturation bubbles due to negative torsional stress are very dynamic, moving erratically along DNA and converting to other topologies (60, 74).

Functions of Top1 and Top2 during Pol I transcription. Both Top1 and Top2 can relax positive and negative supercoiling and are abundant in the nucleolus. The fact that their combined absence results in the inability of polymerases to elongate through the gene shows that either can relieve positive stress in front of advancing polymerases. However, the absence of Top1 resulted in net negative torsion in many active rRNA genes (as manifested by topo-bubbles), while the inactivation of Top2 resulted in slowed transcription elongation, strongly suggesting net positive supercoiling. Top1 is a torque-sensitive topoisomerase and works most efficiently on protein-deficient DNA; Top2 recognizes the double-strand DNA crossovers characteristic of writhed DNA and works better than Top1 on nucleosomal DNA (64). The inability of Top2 to relax the negative topological stress in *top1Δ* thus supports the conclusion that such DNA takes the form of melted rather than supercoiled DNA. Lavelle recently speculated (42) that Top1 would be more effective in relaxing negative torsion behind Pol II, whereas Top2 would be more effective in relax-

ing positive supercoils in front of Pol II. Our findings demonstrate such specialization for Pol I genes.

REFERENCES

1. **Arudchandran, A., et al.** 2000. The absence of ribonuclease H1 or H2 alters the sensitivity of *Saccharomyces cerevisiae* to hydroxyurea, caffeine, and ethyl methanesulphonate: implications for roles of RNases H in DNA replication and repair. Genes Cells **5**:789–802.
2. **Baaklini, I., C. Hraiky, F. Rallu, Y. C. Tse-Dinh, and M. Drolet.** 2004. RNase HI overproduction is required for efficient full-length RNA synthesis in the absence of topoisomerase I in *Escherichia coli*. Mol. Microbiol. **54**:198–211.
3. **Baaklini, I., et al.** 2008. Hypernegative supercoiling inhibits growth by causing RNA degradation. J. Bacteriol. **190**:7346–7356.
4. **Bai, L., T. J. Santangelo, and M. D. Wang.** 2006. Single-molecule analysis of RNA polymerase transcription. Annu. Rev. Biophys. Biomol. Struct. **35**:343–360.
5. **Baxter, J., and J. F. Diffley.** 2008. Topoisomerase II inactivation prevents the completion of DNA replication in budding yeast. Mol. Cell **30**:790–802.
6. **Beckouet, F., et al.** 2008. Two RNA polymerase I subunits control the binding and release of Rrn3 during transcription. Mol. Cell. Biol. **28**:1596–1605.
7. **Boisvert, F. M., Y. W. Lam, D. Lamont, and A. I. Lamond.** 2010. A quantitative proteomics analysis of subcellular proteome localization and changes induced by DNA damage. Mol. Cell Proteomics **9**:457–470.
8. **Boles, T. C., J. H. White, and N. R. Cozzarelli.** 1990. Structure of plectonemically supercoiled DNA. J. Mol. Biol. **213**:931–951.
9. **Bonven, B. J., E. Gocke, and O. Westergaard.** 1985. A high-affinity topoisomerase I binding sequence is clustered at DNase I hypersensitive sites in *Tetrahymena* R-chromatin. Cell **41**:541–551.
10. **Brachmann, C. B., et al.** 1998. Designer deletion strains derived from *Saccharomyces cerevisiae* S288C: a useful set of strains and plasmids for PCR-mediated gene disruption and other applications. Yeast **14**:115–132.
11. **Brill, S. J., S. DiNardo, K. Voelkel-Meiman, and R. Sternglanz.** 1987. Need for DNA topoisomerase activity as a swivel for DNA replication for transcription of rRNA. Nature **326**:414–416.
12. **Brill, S. J., and R. Sternglanz.** 1988. Transcription-dependent DNA supercoiling in yeast DNA topoisomerase mutants. Cell **54**:403–411.
13. **Bryk, M., et al.** 1997. Transcriptional silencing of Ty1 elements in the RDN1 locus of yeast. Genes Dev. **11**:255–269.
14. **Castano, I. B., S. Heath-Pagliuso, B. U. Sadoff, D. J. Fitzhugh, and M. F. Christman.** 1996. A novel family of TRF (DNA topoisomerase I-related function) genes required for proper nuclear segregation. Nucleic Acids Res. **24**:2404–2410.
15. **Cavalli, G., D. Bachmann, and F. Thoma.** 1996. Inactivation of topoisomerases affects transcription-dependent chromatin transitions in rDNA but not in a gene transcribed by RNA polymerase II. EMBO J. **15**:590–597.
16. **Cerritelli, S. M., and R. J. Crouch.** 2009. Ribonuclease H: the enzymes in eukaryotes. FEBS J. **276**:1494–1505.
17. **Christman, M. F., F. S. Dietrich, and G. R. Fink.** 1988. Mitotic recombination in the rDNA of *Saccharomyces cerevisiae* is suppressed by the combined action of DNA topoisomerases I and II. Cell **55**:413–425.
18. **Christman, M. F., F. S. Dietrich, N. A. Levin, B. U. Sadoff, and G. R. Fink.** 1993. The rRNA-encoding DNA array has an altered structure in topoisomerase I mutants of *Saccharomyces cerevisiae*. Proc. Natl. Acad. Sci. U. S. A. **90**:7637–7641.
19. **Dasgupta, A., et al.** 2007. Regulation of rRNA synthesis by TATA-binding protein-associated factor Mot1. Mol. Cell. Biol. **27**:2886–2896.
20. **De Vlaminck, I., et al.** 2010. Torsional regulation of hRPA-induced unwinding of double-stranded DNA. Nucleic Acids Res. **38**:4133–4142.
21. **Drolet, M.** 2006. Growth inhibition mediated by excess negative supercoiling: the interplay between transcription elongation, R-loop formation and DNA topology. Mol. Microbiol. **59**:723–730.
22. **Drygin, D., W. G. Rice, and I. Grummt.** 2010. The RNA polymerase I transcription machinery: an emerging target for the treatment of cancer. Annu. Rev. Pharmacol. Toxicol. **50**:131–156.
23. **El Hage, A., S. L. French, A. L. Beyer, and D. Tollervey.** 2010. Loss of topoisomerase I leads to R-loop mediated transcriptional blocks during rRNA synthesis. Genes Dev. **24**:1546–1558.
24. **Epshtein, V., F. Toulme, A. R. Rahmouni, S. Borukhov, and E. Nudler.** 2003. Transcription through the roadblocks: the role of RNA polymerase cooperation. EMBO J. **22**:4719–4727.
25. **French, S. L., Y. N. Osheim, F. Cioci, M. Nomura, and A. L. Beyer.** 2003. In

exponentially growing *Saccharomyces cerevisiae* cells, rRNA synthesis is determined by the summed RNA polymerase I loading rate rather than by the number of active genes. Mol. Cell. Biol. **23:**1558–1568.

26. **Gadal, O., et al.** 1997. A34.5, a nonessential component of yeast RNA polymerase I, cooperates with subunit A14 and DNA topoisomerase I to produce a functional rRNA synthesis machine. Mol. Cell. Biol. **17:**1787–1795.

27. **Givens, R. M., R. A. Saavedra, and J. A. Huberman.** 1996. Topological complexity of SV40 minichromosomes. J. Mol. Biol. **257:**53–65.

28. **Goto, T., and J. C. Wang.** 1985. Cloning of yeast TOP1, the gene encoding DNA topoisomerase I, and construction of mutants defective in both DNA topoisomerase I and DNA topoisomerase II. Proc. Natl. Acad. Sci. U. S. A. **82:**7178–7182.

29. **Holm, C., T. Goto, J. C. Wang, and D. Botstein.** 1985. DNA topoisomerase II is required at the time of mitosis in yeast. Cell **41:**553–563.

30. **Hontz, R. D., et al.** 2008. Transcription of multiple yeast ribosomal DNA genes requires targeting of UAF to the promoter by Uaf30. Mol. Cell. Biol. **28:**6709–6719.

31. **Hraiky, C., M. A. Raymond, and M. Drolet.** 2000. RNase H overproduction corrects a defect at the level of transcription elongation during rRNA synthesis in the absence of DNA topoisomerase I in *Escherichia coli*. J. Biol. Chem. **275:**11257–11263.

32. **Huertas, P., and A. Aguilera.** 2003. Cotranscriptionally formed DNA:RNA hybrids mediate transcription elongation impairment and transcription-associated recombination. Mol. Cell **12:**711–721.

33. **Huh, W. K., et al.** 2003. Global analysis of protein localization in budding yeast. Nature **425:**686–691.

34. **Iftode, C., Y. Daniely, and J. A. Borowiec.** 1999. Replication protein A (RPA): the eukaryotic SSB. Crit. Rev. Biochem. Mol. Biol. **34:**141–180.

35. **Kim, R. A., and J. C. Wang.** 1989. Function of DNA topoisomerases as replication swivels in *Saccharomyces cerevisiae*. J. Mol. Biol. **208:**257–267.

36. **Kim, R. A., and J. C. Wang.** 1989. A subthreshold level of DNA topoisomerases leads to the excision of yeast rDNA as extrachromosomal rings. Cell **57:**975–985.

37. **Kos, M., and D. Tollervey.** 2010. Yeast pre-rRNA processing and modification occur cotranscriptionally. Mol. Cell **37:**809–820.

38. **Koster, D. A., V. Croquette, C. Dekker, S. Shuman, and N. H. Dekker.** 2005. Friction and torque govern the relaxation of DNA supercoils by eukaryotic topoisomerase IB. Nature **434:**671–674.

39. **Kouzine, F., J. Liu, S. Sanford, H. J. Chung, and D. Levens.** 2004. The dynamic response of upstream DNA to transcription-generated torsional stress. Nat. Struct. Mol. Biol. **11:**1092–1100.

40. **Kouzine, F., S. Sanford, Z. Elisha-Feil, and D. Levens.** 2008. The functional response of upstream DNA to dynamic supercoiling *in vivo*. Nat. Struct. Mol. Biol. **15:**146–154.

41. **Kuo, M. H., and C. D. Allis.** 1999. *In vivo* cross-linking and immunoprecipitation for studying dynamic protein-DNA associations in a chromatin environment. Methods **19:**425–433.

42. **Lavelle, C.** 2008. DNA torsional stress propagates through chromatin fiber and participates in transcriptional regulation. Nat. Struct. Mol. Biol. **15:**123–125.

43. **Leng, F., and R. McMacken.** 2002. Potent stimulation of transcription-coupled DNA supercoiling by sequence-specific DNA-binding proteins. Proc. Natl. Acad. Sci. U. S. A. **99:**9139–9144.

44. **Li, Z., et al.** 2009. Rational extension of the ribosome biogenesis pathway using network-guided genetics. PLoS Biol. **7:**e1000213.

45. **Linskens, M. H., and J. A. Huberman.** 1988. Organization of replication of ribosomal DNA in *Saccharomyces cerevisiae*. Mol. Cell. Biol. **8:**4927–4935.

46. **Liu, L. F., and J. C. Wang.** 1987. Supercoiling of the DNA template during transcription. Proc. Natl. Acad. Sci. U. S. A. **84:**7024–7027.

47. **Ljungman, M., and P. C. Hanawalt.** 1992. Localized torsional tension in the DNA of human cells. Proc. Natl. Acad. Sci. U. S. A. **89:**6055–6059.

48. **Luke, B., et al.** 2008. The Rat1p 5′ to 3′ exonuclease degrades telomeric repeat-containing RNA and promotes telomere elongation in *Saccharomyces cerevisiae*. Mol. Cell **32:**465–477.

49. **Masse, E., and M. Drolet.** 1999. R-loop-dependent hypernegative supercoiling in *Escherichia coli topA* mutants preferentially occurs at low temperatures and correlates with growth inhibition. J. Mol. Biol. **294:**321–332.

50. **Masse, E., P. Phoenix, and M. Drolet.** 1997. DNA topoisomerases regulate R-loop formation during transcription of the rrnB operon in *Escherichia coli*. J. Biol. Chem. **272:**12816–12823.

51. **Merz, K., et al.** 2008. Actively transcribed rRNA genes in *Saccharomyces cerevisiae* are organized in a specialized chromatin associated with the high-mobility group protein Hmo1 and are largely devoid of histone molecules. Genes Dev. **22:**1190–1204.

52. **Muller, M., R. Lucchini, and J. M. Sogo.** 2000. Replication of yeast rDNA initiates downstream of transcriptionally active genes. Mol. Cell **5:**767–777.

53. **Muller, M. T., W. P. Pfund, V. B. Mehta, and D. K. Trask.** 1985. Eukaryotic type I topoisomerase is enriched in the nucleolus and catalytically active on ribosomal DNA. EMBO J. **4:**1237–1243.

54. **Murchie, A. I., R. Bowater, F. Aboul-ela, and D. M. Lilley.** 1992. Helix opening transitions in supercoiled DNA. Biochim. Biophys. Acta **1131:**1–15.

55. **Oakes, M., I. Siddiqi, L. Vu, J. Aris, and M. Nomura.** 1999. Transcription factor UAF, expansion and contraction of ribosomal DNA (rDNA) repeats, and RNA polymerase switch in transcription of yeast rDNA. Mol. Cell. Biol. **19:**8559–8569.

56. **Osheim, Y. N., et al.** 2004. Pre-18S rRNA is structurally compacted into the SSU processome prior to being cleaved from nascent transcripts in *Saccharomyces cerevisiae*. Mol. Cell **16:**943–954.

57. **Osheim, Y. N., S. L. French, M. L. Sikes, and A. L. Beyer.** 2009. Electron microscope visualization of RNA transcription and processing in *Saccharomyces cerevisiae* by Miller chromatin spreading. Methods Mol. Biol. **464:**55–69.

58. **Parvin, J. D., and P. A. Sharp.** 1993. DNA topology and a minimal set of basal factors for transcription by RNA polymerase II. Cell **73:**533–540.

59. **Prunell, A.** 1998. A topological approach to nucleosome structure and dynamics: the linking number paradox and other issues. Biophys. J. **74:**2531–2544.

60. **Randall, G. L., L. Zechiedrich, and B. M. Pettitt.** 2009. In the absence of writhe, DNA relieves torsional stress with localized, sequence-dependent structural failure to preserve B-form. Nucleic Acids Res. **37:**5568–5577.

61. **Roca, J., and J. C. Wang.** 1994. DNA transport by a type II DNA topoisomerase: evidence in favor of a two-gate mechanism. Cell **77:**609–616.

62. **Saavedra, R. A., and J. A. Huberman.** 1986. Both DNA topoisomerases I and II relax 2 micron plasmid DNA in living yeast cells. Cell **45:**65–70.

63. **Saffer, L. D., and O. L. Miller, Jr.** 1986. Electron microscopic study of *Saccharomyces cerevisiae* rDNA chromatin replication. Mol. Cell. Biol. **6:**1148–1157.

64. **Salceda, J., X. Fernandez, and J. Roca.** 2006. Topoisomerase II, not topoisomerase I, is the proficient relaxase of nucleosomal DNA. EMBO J. **25:**2575–2583.

65. **Schoeffler, A. J., and J. M. Berger.** 2008. DNA topoisomerases: harnessing and constraining energy to govern chromosome topology. Q. Rev. Biophys. **41:**41–101.

66. **Schultz, M. C., S. J. Brill, Q. Ju, R. Sternglanz, and R. H. Reeder.** 1992. Topoisomerases and yeast rRNA transcription: negative supercoiling stimulates initiation and topoisomerase activity is required for elongation. Genes Dev. **6:**1332–1341.

67. **Shaw, R. J., and D. Reines.** 2000. *Saccharomyces cerevisiae* transcription elongation mutants are defective in PUR5 induction in response to nucleotide depletion. Mol. Cell. Biol. **20:**7427–7437.

68. **Smith, J. S., E. Caputo, and J. D. Boeke.** 1999. A genetic screen for ribosomal DNA silencing defects identifies multiple DNA replication and chromatin-modulating factors. Mol. Cell. Biol. **19:**3184–3197.

69. **Stupina, V. A., and J. C. Wang.** 2004. DNA axial rotation and the merge of oppositely supercoiled DNA domains in *Escherichia coli*: effects of DNA bends. Proc. Natl. Acad. Sci. U. S. A. **101:**8608–8613.

70. **Thrash, C., A. T. Bankier, B. G. Barrell, and R. Sternglanz.** 1985. Cloning, characterization, and sequence of the yeast DNA topoisomerase I gene. Proc. Natl. Acad. Sci. U. S. A. **82:**4374–4378.

71. **Tous, C., and A. Aguilera.** 2007. Impairment of transcription elongation by R-loops *in vitro*. Biochem. Biophys. Res. Commun. **360:**428–432.

72. **Travers, A., and G. Muskhelishvili.** 2007. A common topology for bacterial and eukaryotic transcription initiation? EMBO Rep. **8:**147–151.

73. **Treuner, K., U. Ramsperger, and R. Knippers.** 1996. Replication protein A induces the unwinding of long double-stranded DNA regions. J. Mol. Biol. **259:**104–112.

74. **Trovato, F., and V. Tozzini.** 2008. Supercoiling and local denaturation of plasmids with a minimalist DNA model. J. Phys Chem. B **112:**13197–13200.

75. **Wang, J. C.** 2002. Cellular roles of DNA topoisomerases: a molecular perspective. Nat. Rev. Mol. Cell. Biol. **3:**430–440.

76. **Wang, J. C., and A. S. Lynch.** 1993. Transcription and DNA supercoiling. Curr. Opin. Genet. Dev. **3:**764–768.

77. **Warner, J. R.** 1999. The economics of ribosome biosynthesis in yeast. Trends Biochem. Sci. **24:**437–440.

78. **Wery, M., S. Ruidant, S. Schillewaert, N. Lepore, and D. L. Lafontaine.** 2009. The nuclear poly(A) polymerase and exosome cofactor Trf5 is recruited cotranscriptionally to nucleolar surveillance. RNA **15:**406–419.

79. **Winzeler, E. A., et al.** 1999. Functional characterization of the *Saccharomyces cerevisiae* genome by gene deletion and parallel analysis. Science **285:**901–906.

80. **Wu, H. Y., S. H. Shyy, J. C. Wang, and L. F. Liu.** 1988. Transcription generates positively and negatively supercoiled domains in the template. Cell **53:**433–440.

81. **Zhang, H., J. C. Wang, and L. F. Liu.** 1988. Involvement of DNA topoisomerase I in transcription of human rRNA genes. Proc. Natl. Acad. Sci. U. S. A. **85:**1060–1064.

82. **Zhang, Y., M. L. Sikes, A. L. Beyer, and D. A. Schneider.** 2009. The Paf1 complex is required for efficient transcription elongation by RNA polymerase I. Proc. Natl. Acad. Sci. U. S. A. **106:**2153–2158.